Organohalide Perovskites are Fast Ionic Conductors

*Nuria Vicente and Germà Garcia-Belmonte**

Fast ionic conductors constitute a family of materials exhibiting high values of the ionic conductivity while their crystal structure remains rather rigid. Perovskite-like compounds are known to be good ionic conductors with applications as solid electrolytes. In hybrid halide perovskites both intrinsic (native) and extrinsic defect migration are regarded to occur. Ion diffusivity analysis is inherently ambiguous in all-solid-state configurations because of the multicomponent environment. Here, a liquid electrolyte in contact to the perovskite material forms a reservoir of Li^+ that is forced to intercalate and migrate within the perovskite electrode. This approach decouples different contributions to transport in such a way that ion diffusion kinetics is easily accessible by means of impedance methods. The room-temperature chemical diffusion coefficient of lithium ion within the perovskite lattice exhibits values as high as $D_\mu \approx 10^{-7}$ cm^2 s^{-1}, which implies conductivities within the range of 10^{-3} Ω^{-1} cm^{-1} for highly lithiated electrodes. This confirms the superionic intrinsic property of organohalide perovskites from a direct and unambiguous measurement that does not rely upon simulation tools.

Fast ionic conductors (also known as superionic conductors) constitute a family of materials exhibiting high values of the ionic conductivity or diffusivity.[1,2] Their principal feature is the ability to keep the crystal structure rather frozen while permitting the migration of ionic species. Fast ionic conductors are of particular interest for technological applications in the field of solid electrolytes for electrochemical devices such as batteries, supercapacitors, sensors, electrochromic windows, and ionic membranes for fuel cells. Typically, ionic conductivity lies within the range of 10^{-4} to 10^{-1} Ω^{-1} cm^{-1} at room temperature to consider a material as superionic conductor. Some fast ionic conductors also exhibit prominent electronic conductivity and are known as mixed ionic–electronic conductors. Many perovskite-type oxides belong to this class of materials and have well-known applications in solid-oxide fuel cells and oxygen permeation membranes.[3,4] Even halide perovskites of the type $CsPbX_3$ (X = Cl, Br) are also known to be good ionic conductors.[5] Native defects in hybrid lead halide perovskite materials are known to migrate within the perovskite lattice because of the soft character of the compounds. First-principles computational studies have identified facile migration of iodine anions through a vacancy-assisted mechanism, and also long-range displacement of the organic cation, although different calculated activation energies have been reported.[6–8] These simulations observe presence in equilibrium of several ionic vacancies and interstitials (I^-, Br^-, Pb^{2+}, and $CH_3NH_3^+$) at room temperature. Also, extrinsic defects as hydrogen has been studied by first principles.[9] However, there is no clear agreement concerning the ion diffusion time scale or the dominant ionic species. Whereas some studies have reported diffusivity values of native defects in organohalide perovskites of the order of those encountered in common solid-state ionic conductors, $D \approx 10^{-12}$ cm^2 s^{-1},[7,10,11] other analyses give much faster ion migration coefficients $D \approx 10^{-8}$ to 10^{-7} cm^2 s^{-1}.[12,13] Despite the recognized need for knowing about the kinetics of ion migration, the complex defect chemistry exhibited by organohalide perovskites makes it difficult discerning about the diffusivity of specific mobile ions.

Because the determination of defect diffusivities in perovskite films is inherently complex, here an approach is proposed that takes advantage of the intercalation and migration of extrinsic lithium ions into methylammonium lead bromide perovskite to unambiguously extract diffusivity values. Instead of working on all-solid-state configurations, a reservoir of Li^+ makes part of the liquid electrolyte in contact to the perovskite material. In this configuration (**Figure 1**a), Li^+ is forced to intercalate and migrate within the perovskite electrode in such a way that the ion diffusion kinetics is easily accessible by means of impedance methods. Provided the mixed conduction character of organohalide perovskites with very high electronic mobilities,[14] our approach decouples the electronic from the ionic transport thereby avoiding the intrinsic ambiguity of solid-state methods. This is feasible because both electronic and ionic densities increase by the same amount upon intercalation, in such a way that electronic conductivity always exceeds the ionic conductivity. It is the slowest charge carrier that determines the kinetics.

In the present work, the hybrid perovskite $CH_3NH_3PbBr_3$ has been utilized as active material for the intercalation electrode in a lithium-ion half-battery setup (Figure 1a). Easy Li^+ intercalation is related to the framework of corner-connected MX_6 (M = Pb, X = Br) octahedrons with organic methylammonium cations located between them.[15] The hybrid halide perovskite behaves as a compact structure in which the dimensionality of Li^+ transport is 3D similarly to that occurring for

N. Vicente, Prof. G. Garcia-Belmonte
Institute of Advanced Materials (INAM)
Universitat Jaume I
12006 Castelló, Spain
E-mail: garciag@uji.es

The ORCID identification number(s) for the author(s) of this article can be found under https://doi.org/10.1002/aenm.201700710.

DOI: 10.1002/aenm.201700710

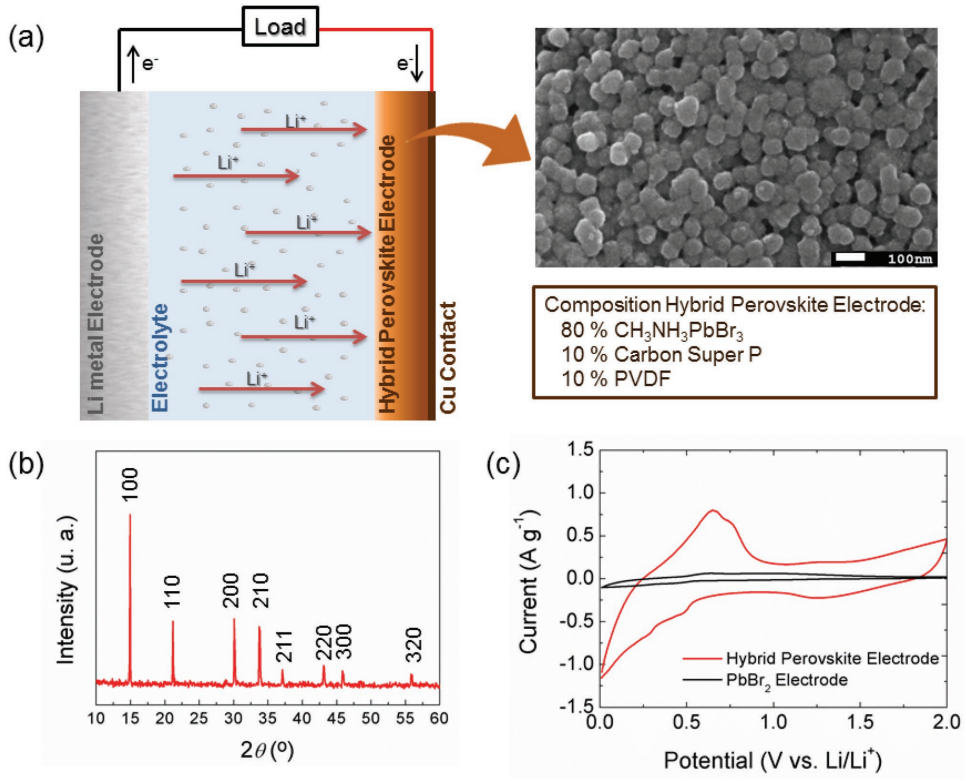

Figure 1. a) Schema of half-battery setup indicating the composition of the hybrid perovskite electrode deposited on a cooper contact. SEM image showing the compact structure formed by $CH_3NH_3PbBr_3$ particles. b) X-ray diffraction patterns of $CH_3NH_3PbBr_3$. The vertical peaks correspond to the $CH_3NH_3PbBr_3$ cubic phase signals. c) Stable cyclic voltammetry of $CH_3NH_3PbBr_3$ electrodes after the first four cycles, compared to the electrochemical activity of $PbBr_2$ electrodes.

intercalation spinel compounds such as $LiMn_2O_4$. Moreover, perovskite electrodes allow checking ion diffusion dynamics of extrinsic defects (Li^+) in a fully controllable way. Hence, our strategy avoids the inherent uncertainty found in analyzing native defect migration in a multicomponent environment. It is observed that room-temperature chemical diffusion coefficient of lithium ion within the perovskite lattice exhibits values as high as $D_\mu \approx 10^{-7}$ cm^2 s^{-1}, which implies ionic conductivities within the range of 10^{-3} Ω^{-1} cm^{-1} for highly lithiated electrodes. This confirms the fast ionic conductor character of hybrid perovskite materials from a direct and unambiguous measurement that does not rely upon simulation tools.

Perovskite-based electrodes are prepared as described in the Experimental Section and recently reported.[16] XRD analysis confirms the pure perovskite crystallographic phase (Figure 1b). Electrodes comprise $CH_3NH_3PbBr_3$ composed of 65 nm average size particles, conductive carbon black, and poly(vinylidenedifluoride) binder (PVDF, Sigma-Aldrich), with a 80:10:10 weight ratio, deposited on Cu foils (Figure 1a). The use of carbon black ensures a good electronic connection between Cu and the perovskite particles. The driving force for Li^+ transport relates to the ion chemical potential gradient $\Delta\mu$ that establishes the electrode potential as $eV = -[\mu(x) - \mu_{ref}]$, with e being the positive elementary charge, x the molar concentration in $Li_xCH_3NH_3PbBr_3$, and μ_{ref} the Li-metal electrode potential reference. For testing electrochemical response, perovskite-based anodes were monitored by cyclic voltammetry (CV; see the Experimental Section for details). Figure 1c shows stable CV signal that does not change significantly through continuous cycling.[16] It confirms a good reversibility for the electrode material. The reaction peaks related to Li^+ insertion are observed at 0.49 and 0.27 V versus Li/Li^+, and the Li^+ extraction from the matrix produces two peaks in the delithiation current at 0.65 and 0.75 V versus Li/Li^+. Contrary to that occurring for conducting polymer[17] or redox molecule modified electrodes,[18] in which the energy landscape of electronic states dictates the electrochemical response, perovskite-based anodes are driven by the ionic energetics. As recently reported, $CH_3NH_3PbBr_3$ electrodes exhibit a highly reversible lithium uptake and release without severe distortion of the perovskite lattice (topotactic intercalation). Even the basic band structure remains unaltered for the potential window of interest.[16] As observed in Figure 1c, electrodes comprising perovskite precursors ($PbBr_2$) have no electrochemical activity in comparison to perovskite-based electrodes. Hence, the electrochemical setup used here constitutes an excellent approach to investigate ion diffusion through the perovskite lattice.

Electrochemical impedance spectroscopy (EIS) analysis is performed potentiostatically at different charge states after the first cycles, for discharging (lithiation) steps of 50 mC. Galvanostatic lithiation profile of electrodes within the voltage range 1.80–0.01 V versus Li/Li^+ during EIS measurements is shown in **Figure 2**a. See the recent report on charge/discharge curves and rate capability.[16] The impedance plots in Figure 2b

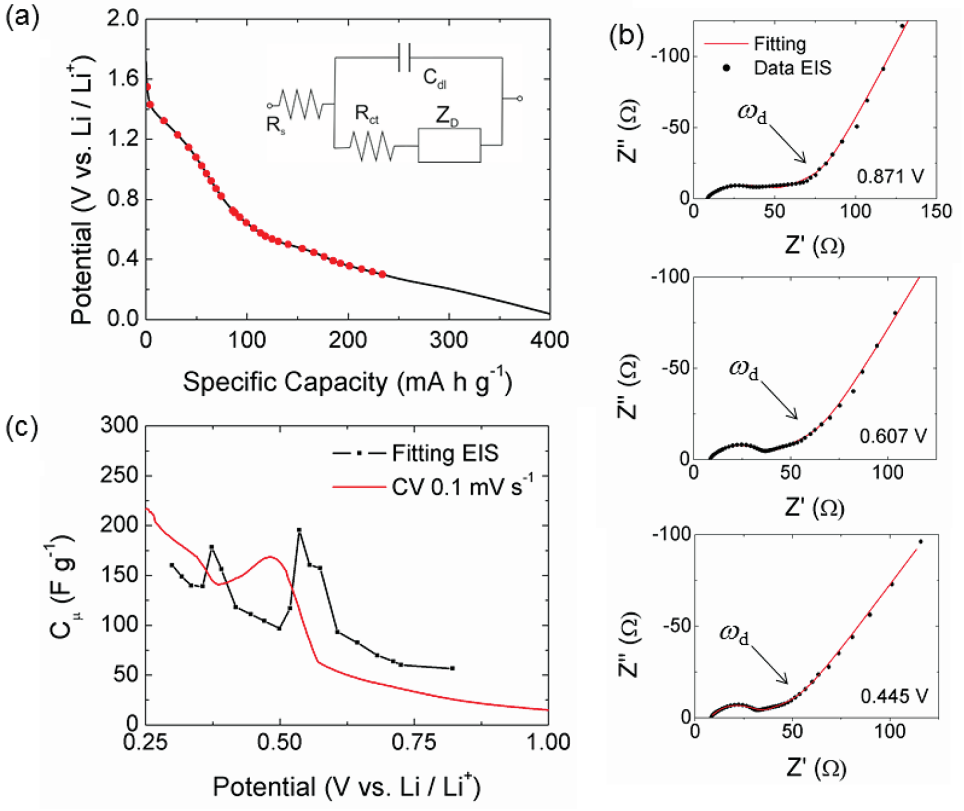

Figure 2. Electrochemical impedance analysis. a) Selected potentials and charge state of the electrode lithiation process for in situ EIS analysis during the lithiation process. Inset: Randles' equivalent circuit used in the EIS fitting. b) Impedance spectroscopy response of $CH_3NH_3PbBr_3$ electrodes at different steady-state voltages as indicated. The solid line corresponds to fits using the equivalent circuit. The diffusion response frequency ω_d is marked. c) C_μ calculated from different data: EIS and cyclic voltammetry plotted versus potential during lithiation process.

consist of three well-defined parts: the high-frequency semicircle related to electrode/electrolyte processes, the middle frequency diffusion pattern, and an inclined low-frequency line in response to the electrochemical charging. The impedance spectra could be modeled by means of a well-known Randles' equivalent circuit as shown in the inset of Figure 2a. The equivalent circuit includes a parallel subcircuit of R_{ct} and C_{dl} that accounts for the polarization charge-transfer resistance and the double-layer capacitance associated with the electrode/electrolyte interface. At high frequencies, a rather voltage- and electrode-thickness-independent arc is found with $C_{dl} \approx 2.8$ mF g^{-1} ($C_{dl} \approx 10$ µF cm^{-2}; see Figure S1 in the Supporting Information) and $R_{ct} \approx 0.14$ Ω g ($R_{ct} \approx 20.16$ Ω cm^2). These trends and values allow readily connecting them to mechanisms occurring at the outer electrode/electrolyte interface. In addition, the series resistance accounts for the ohmic resistance $R_s \approx 0.04$ Ω g ($R_s \approx 5.6$ Ω cm^2).

The intermediate- and low-frequency impedance response points to a diffusive-capacitive behavior that depends on the voltage (charging) state. This performance informs on the electrode ability of varying its capacity because of the intercalation of Li^+ in the perovskite structure. By examining this behavior, it is possible to know how fast ions can be inserted into or withdrawn (extracted) from a rather stable host crystal lattice. The impedance model used here corresponds to the classical spatially restricted diffusion element, which exhibits the so-called anomalous diffusion response, Z_D in the inset of Figure 2a.[19] This scheme assumes large enough electronic conductivity so as to render Li^+ diffusion as determining parameter of the charging process. This is expected to be the case provided the high electronic mobility reported for solar perovskite materials.[14] Diffusion impedances undergo a pattern change at a certain characteristic frequency ω_d at which a transition between a Warburg- to a capacitive-like behavior is observed.[20,21] The frequency ω_d is located near the elbow of the impedance plot, as marked in Figure 2b, and relates to the chemical diffusion coefficient D_μ as

$$\omega_d = \frac{D_\mu}{L^2} \tag{1}$$

Here, L accounts for the thickness of the electrode. The finite-length diffusion element is given by

$$Z_D = R_d \left(i\omega/\omega_d\right)^{-\gamma/2} \coth\left[\left(i\omega/\omega_d\right)^{-\gamma/2}\right] \tag{2}$$

with ω being the angular frequency and $i = \sqrt{-1}$. R_d is the resistance associated with the ionic diffusion, and γ relates to the deviation from the ideal spatially restricted diffusion impedance ($\gamma = 1$). The anomalous diffusion mechanism ($\gamma < 1$) is expected to occur in a multiphasic matrix.[22] Models based on spatially restricted ion diffusion were proposed to account for intermediate-frequency distortions relaying on a distribution of

diffusion lengths[23] or electronic transport limitations.[24] Diffusion of ions gives rise to distinctive impedance patterns characterized by Warburg-like responses as $Z \propto (i\omega)^{-\gamma/2}$ at intermediate frequencies. At lower frequencies, the electrode charging is manifested in the capacitive response of the impedance through the chemical capacitance $C_\mu = e^2 N\, dx/d\mu$ element, with N being the total density of intercalation ion sites in the perovskite lattice. It is related to the characteristic frequency as

$$\omega_d = \frac{1}{R_d C_\mu} \tag{3}$$

By fitting the equivalent circuit in the inset of Figure 2a to the impedance data in Figure 2b for different voltage stages during lithiation process, it is found that the diffusion resistance decreases with voltage, from 0.18 Ω g at 1.20 V down to 0.08 Ω g at 0.30 V. It is also checked for consistency that the chemical capacitance extracted from impedance and that derived from CV as $C_\mu = -dQ/dV$ yields similar values (Figure 2c), with a voltage shift in the peak position related to kinetic limitations in the case of large-amplitude, out-of-equilibrium techniques such as CV at usual scan rates.

Some caution words are in order here about the applicability of the previously outlined diffusion model. The extraction of the chemical diffusion coefficient D_μ using Equation (1) relays on a proper determination of the diffusion length that, in certain experimental conditions, does not coincide with the electrode thickness L. If the electrolyte penetrates the electrode and wets the active particles, the effective diffusion length in the solid state may be significantly reduced $L_{eff} << L$, giving rise to large overestimations in D_μ. The so-called porous impedance model allows addressing these last cases.[23–25] Hence, it is a matter of experimental check to discern if $L_{eff} \approx L$, in such a way that the finite-length diffusion mechanism in Equation (2) can be exploited to determine D_μ. Here electrodes with different thickness, by varying the weight of the active material, have been tested by impedance.

As the perovskite lithiation progresses, specific capacity values as high as 400 mA h g^{-1} are reached (Figure 2a), which implies a Li-ion concentration as high as 10^{21} cm^{-3}, given perovskite densities approximately equal to 4.16 g cm^{-3}. The host matrix becomes fully lithiated at potentials below 0.5 V, as discussed very recently.[16] It is worth determining the chemical diffusion coefficient in Equation (1), where the diffusion characteristic frequency is extracted from long-range Li^+ displacements corresponding to the thickness of the electrode. The variation of the diffusion characteristic frequency ω_d with voltage is shown in **Figure 3**a. One can observe that ω_d appears to be rather voltage independent but exhibits a clear correlation with the electrode thickness in agreement with Equation (1). A close examination of the average values of ω_d as a function of L allows verifying the validity of our approach (Figure 3b). Here, it has been checked that fitting the expression $\omega_d = D_\mu L^{-n}$ yields a value for the thickness coefficient equaling $n = 2.8 \pm 0.6$. This agrees with the thickness dependence predicted by Equation (1) as $n \approx 2$ within the experimental error. This observation allows extracting $D\mu = (2.8 \pm 1.0) \times 10^{-7}$ cm^2 s^{-1} given the strong correlation between ω_d and the electrode thickness. An additional point reinforcing that $L_{eff} \approx L$ is the

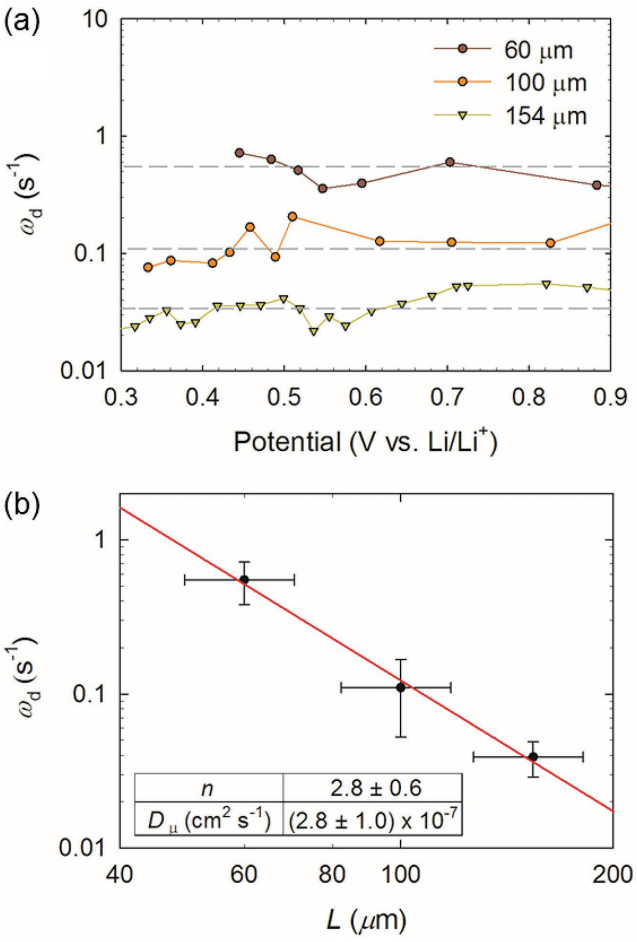

Figure 3. a) Variation of the diffusion characteristic frequency ω_d as a function of the voltage for three different electrode thicknesses. Dashed lines signals average frequency values. b) Dependence of the diffusion characteristic frequency on the electrode thickness. The used fitting function $\omega_d = D_\mu L^{-n}$ provides values for $D_\mu = (2.8 \pm 1.0) \times 10^{-7}$ cm^2 s^{-1} and thickness coefficient $n = 2.8 \pm 0.6$, considering the experimental error.

electrode-thickness-independent trend exhibited by the double-layer capacitance. As shown in Figure S1 (Supporting Information), C_{dl} is always situated around typical values on the order of μF cm^{-2}, not correlated with L at all. This is in contradiction with that derived from the porous electrode model in which the electrolyte/electrode interface is extended within the matrix producing double-layer capacitances largely exceeding μF cm^{-2} values.[26] Moreover, one would expect strong correlations between C_{dl} and the electrode thickness for the porous electrode model. These trends have neither been observed in our samples.

Diffusivity attains rather voltage-independent values in the range of $D_\mu \approx 10^{-7} cm^2$ s^{-1}. This high lithium diffusivity corresponds to conductivities within the range of 10^{-3} Ω^{-1} cm^{-1} for highly lithiated electrodes. It is checked here that the procedure to determine the chemical diffusion coefficient is consistent with the electrode thickness variation. This fact allows us to discard relating ω_d to the perovskite particle size (65 nm) and verifies the proposed diffusion model in Equation (2) , with L equaling the thickness of the host matrix.

To sum up, our findings unambiguously show that lead halide perovskites can be regarded as fast ionic conductors with large diffusion coefficients. The approach followed here, using an electrolyte/electrode contact, allows decoupling electronic from ionic transport. This avoids the inherent ambiguity of all-solid-state experimental techniques. The room-temperature chemical diffusion coefficient of Li^+ within the perovskite lattice exhibits values as high as $D_\mu \approx 10^{-7}$ cm^2 s^{-1}, which implies conductivities within the range of 10^{-3} Ω^{-1} cm^{-1} for highly lithiated electrodes. The proved superionic intrinsic property of organohalide perovskites opens new room for devising applications and devices in which fast ionic migration is an essential requirement.

Experimental Section

Perovskite material were synthesized by slow evaporation of *N*,*N*-dimethylformamide (DMF, Sigma-Aldrich) in a solution containing stoichiometric amounts of lead bromide ($PbBr_2$, TCI) and methylammonium bromide (CH_3NH_3Br, >98% TCI) 1 M in DMF, as recently reported.[16] Solid precipitated becomes orange at the end of the reaction. A Bruker AXS-D4 Endeavor Advance X-ray diffractometer using Cu Kα, wavelength $\lambda = 1.5406$ Å, is employed in XRD to confirm the pure perovskite crystallographic structure.

The working anode electrode (Figure 1a) was prepared by mixing $CH_3NH_3PbBr_3$ composed of 65 nm average size particles, conductive carbon black and PVDF binder (Sigma-Aldrich) with a 80:10:10 weight ratio, and *N*-methyl-2-pyrrolidone as solvent.[16] Also, the blank electrode comprising $PbBr_2$ contains the same weight ratio (80:10:10). The slurry was coated on a copper foil by Dr. Blade and dried at 100 °C overnight. Working electrodes for electrochemical analysis were made up of composite material slices with a diameter of 10 mm using Swagelok-type cells. Li metal foil was used as the counter and reference electrode (Figure 1a), and an electrolyte-soaked, microporous monolayer membrane (Celgard 2500) is employed as a separator. The electrolyte is 1 M of hexafluorophosphate lithium salt ($LiPF_6$, Sigma-Aldrich) dissolved in ethylene carbonate, ethyl-methyl carbonate, and dimethyl carbonate (EC:EMC:DMC, Sigma-Aldrich) with 1:1:1 v/v. Cell assembly was carried out in an N_2 filled glovebox. For electrochemical characterization, a PGSTAT-30 potentiostat from AUTOLAB equipped with an impedance module was employed. CV was performed in the voltage range from 0.01 to 2.00 V with a rate of 5 mV s^{-1}. After the first cycle, the second discharge EIS test was carried out potentiostatically every 50 mC of discharge (Figure 2a), with an amplitude perturbation of 10 mV in the frequency range of 1 MHz to 10 mHz. The approximation to the different measuring voltages was galvanostatically controlled at 50 mA g^{-1} to ensure the quasi-equilibrium state of the electrode. All the data are normalized to the load $CH_3NH_3PbBr_3$ mass.

Supporting Information

Supporting Information is available from the Wiley Online Library or from the author.

Acknowledgements

The authors acknowledge the financial support by Generalitat Valenciana under Prometeo Project (PROMETEO/2014/020) and Ministerio de Economía y Competitividad (MINECO) of Spain under Project (MAT2016-76892-C3-1-R). N.V. acknowledges University Jaume I through FPI Fellowship Program (PREDOC/2015/54) and Project (UJI-B2016-35). SCIC from Universitat Jaume I is acknowledged. The authors also acknowledge Celgard for supplying separator membranes.

Conflict of Interest

The authors declare no conflict of interest.

Keywords

intercalation, impedance, ion conduction, lithium-ion diffusion, perovskites

Received: March 15, 2017
Revised: May 15, 2017
Published online:

[1] H. L. Tuller, P. K. Moon, *Mater. Sci. Eng. B* **1988**, *1*, 171.
[2] S. Adams, J. Swenson, *Phys. Rev. Lett.* **2000**, *84*, 4144.
[3] M. Li, M. J. Pietrowski, R. A. De Souza, H. Zhang, I. M. Reaney, S. N. Cook, J. A. Kilner, D. C. Sinclair, *Nat. Mater.* **2014**, *13*, 31.
[4] H. Hayashi, H. Inaba, M. Matsuyama, N. G. Lan, M. Dokiya, H. Tagawa, *Solid State Ionics* **1999**, *122*, 1.
[5] J. Mizusaki, K. Arai, K. Fueki, *Solid State Ionics* **1983**, *11*, 203.
[6] J. M. Azpiroz, E. Mosconi, J. Bisquert, F. De Angelis, *Energy Environ. Sci.* **2015**, *8*, 2118.
[7] C. Eames, J. M. Frost, P. R. F. Barnes, B. C. O'Regan, A. Walsh, M. S. Islam, *Nat. Commun.* **2015**, *6*, 7497.
[8] J. Haruyama, K. Sodeyama, L. Han, Y. Tateyama, *J. Am. Chem. Soc.* **2015**, *137*, 10048.
[9] D. A. Egger, L. Kronik, A. M. Rappe, *Angew. Chem. Int. Ed.* **2015**, *54*, 12437
[10] M. Bag, L. A. Renna, R. Y. Adhikari, S. Karak, F. Liu, P. M. Lahti, T. P. Russell, M. T. Tuominen, D. Venkataraman, *J. Am. Chem. Soc.* **2015**, *137*, 13130.
[11] G. Richardson, S. E. J. O'Kane, G. Niemann Ralf, T. A. Peltola, J. M. Foster, P. J. Cameron, A. B. Walker, *Energy Environ. Sci.* **2016**, *9*, 1476.
[12] T.-Y. Yang, G. Gregori, N. Pellet, M. Grätzel, J. Maier, *Angew. Chem., Int. Ed.* **2015**, *127*, 8016.
[13] O. Almora, A. Guerrero, G. Garcia-Belmonte, *Appl. Phys. Lett.* **2016**, *108*, 043903.
[14] S. D. Stranks, G. E. Eperon, G. Grancini, C. Menelaou, M. J. P. Alcocer, T. Leijtens, L. M. Herz, A. Petrozza, H. J. Snaith, *Science* **2013**, *342*, 341.
[15] H.-R. Xia, W.-T. Sun, L.-M. Peng, *Chem. Commun.* **2015**, *51*, 13787.
[16] N. Vicente, G. Garcia-Belmonte, *J. Phys. Chem. Lett.* **2017**, *8*, 1371.
[17] J. Bisquert, G. Garcia-Belmonte, J. García-Cañadas, *J. Chem. Phys.* **2004**, *120*, 6726.
[18] D. A. Miranda, P. R. Bueno, *Phys. Chem. Chem. Phys.* **2016**, *18*, 25984.
[19] J. Bisquert, A. Compte, *J. Electroanal. Chem.* **2001**, *499*, 112.
[20] G. Garcia-Belmonte, Z. Pomerantz, J. Bisquert, J.-P. Lellouche, A. Zaban, *Electrochim. Acta* **2004**, *49*, 3413.
[21] J. García-Cañadas, F. Fabregat-Santiago, I. Porqueras, C. Person, J. Bisquert, G. Garcia-Belmonte, *Solid State Ionics* **2004**, *175*, 521.
[22] J. Bisquert, G. Garcia-Belmonte, A. Pitarch, *ChemPhysChem* **2003**, *4*, 287.
[23] M. D. Levi, D. Aurbach, *J. Phys. Chem. B* **2004**, *108*, 11693.
[24] J. P. Meyers, M. Doyle, R. M. Darling, J. Newman, *J. Electrochem. Soc.* **2000**, *147*, 2930.
[25] J. Bisquert, G. Garcia-Belmonte, F. Fabregat-Santiago, A. Compte, *Electrochem. Commun.* **1999**, *1*, 429.
[26] M. Haro, N. Vicente, G. Garcia-Belmonte, *Adv. Mater. Interfaces* **2015**, *2*, 1500369.

